Eur. Phys. J. D **10**, 327–340 (2000)

THE EUROPEAN PHYSICAL JOURNAL D

EDP Sciences

Doubly excited states in the negative hydrogen ion

A. Bürgers[a] and E. Lindroth

Atomfysik, Stockholms Universitet, Frescativägen 24, 104 05 Stockholm, Sweden

Received 10 March 1999 and Received in final form 18 October 1999

Abstract. We present a detailed analysis of doubly excited resonances in H^- of both $^1S^e$ and $^1P^o$ symmetry. Both resonance positions and total widths for auto-detachment are calculated using complex coordinate scaling in a Sturmian-type basis in perimetric coordinates. The resonances are classified by approximate quantum numbers with help of their Lewis structures. For the first time, a new class of shape resonances is reported which can be understood as resulting from couplings between different adiabatic potentials with both binding and repulsive character. In addition, we present an analysis of the so called mass polarisation term which gives rise to specific isotope shifts.

PACS. 31.15.Ar Ab initio calculations – 31.50.+w Excited states – 32.80.Dz Autoionization

1 Introduction

Negative ions are known to be very sensitive for electron correlation. This is especially true for their doubly excited states, where the electron-electron interaction within the outer pair of electrons is of the same order of magnitude as the electron-nucleus interaction. The most simple negative ion is H^- which has been studied excessively both experimentally and theoretically [1–14].

Only the ground state of H^- is truly bound. There are no singly excited states, but there exist doubly excited states which are embedded in the continuous part of the spectrum of the hydrogen atom and can be detected as resonances in electron-hydrogen scattering or in the photo-detachment cross-section of H^-. Neglecting relativistic effects, it was shown that resonances can form dipole series converging exponentially to each threshold [15]. Crucial for this derivation is the strong degeneracy of the hydrogenic parent atom which leads to the possibility of forming a permanent dipole in whose field the additional electron can be bound. If the potential is too weak to hold a dipole series, there is still the possibility of forming a finite number of resonances. The most prominent example for such a state is the well known $^1P^o$ shape resonance just above the $N = 2$ hydrogenic threshold.

Relativistic effects are negligible for resonances well below the corresponding threshold. However, if their binding energy with respect to this threshold becomes comparable to the fine structure splitting of the hydrogenic parent term the resonances will be shifted significantly and the series will terminate. Calculations have shown that below the $N = 2$ threshold the $^1S^e$ series has four and the $^1P^o$ series three members [16,17].

[a] e-mail: burgers@atom.msi.se

Recent measurements on H^- and D^- [18,19] shifted the interest to the so called mass polarisation term. The full non-relativistic Hamiltonian for a two electron atom or ion reads (in atomic units, $e = m_e = \hbar = 4\pi\varepsilon_0 = 1$)

$$\mathcal{H} = \frac{\mathbf{p}_1^2}{2\mu} + \frac{\mathbf{p}_2^2}{2\mu} + \frac{\mathbf{p}_1 \cdot \mathbf{p}_2}{M} - \frac{Z}{r_1} - \frac{Z}{r_2} + \frac{1}{r_{12}} \qquad (1)$$

where M is the mass of the nucleus and μ the reduced mass of the electron-nucleus system, $\mu = (Mm_e)/(M + m_e)$. In most calculations, the limit $M \to \infty$ is taken and the mass polarisation term is neglected. However, it is important when comparisons between calculations and measurements are made or when different isotopes of the same element are compared. It describes a specific energy shift which is beyond a re-scaling of the energy by introducing the correct reduced mass μ.

The mass polarisation term (or specific mass shift) has influence on both the resonance position E_R and on its width Γ. Viewing the resonance energy as a complex entity $E_{res} = E_R - i\Gamma/2$, the (measured) energy E_{res}^M for an isotope with nuclear mass M and the (calculated) energy E_{res}^∞ for infinite nuclear mass are connected through

$$E_{res}^M = \frac{\mu}{m_e} E_{res}^\infty + \Delta E_M \, . \qquad (2)$$

The specific mass shift ΔE_M is defined by

$$\Delta E_M = \frac{\langle\langle \mathbf{p}_1 \cdot \mathbf{p}_2 \rangle\rangle}{M} \qquad (3)$$

where $\langle\langle . \rangle\rangle$ denotes a complex matrix element (see next section). Since the binding energies are given with respect to the three-particle breakup threshold (*i.e.* the ionisation energy of H), $\mathrm{Re}\,\Delta E_M > 0$ means that the resonance is shifted closer towards threshold, *i.e.* its binding energy decreases, while $\mathrm{Im}\,\Delta E_M > 0$ means that its width decreases

and the resonance is stabilized by the movement of the nucleus. While reference [18] reported a small specific mass shift which is consistent with theory, a comparatively large mass shift was reported in reference [19] which was inconsistent with theoretical calculations.

2 Computational method

2.1 Basis set expansion

We calculate the resonance parameters by expanding the full two-electron wave function as

$$\Psi^{\pi}_{L,M}(\mathbf{r}_1,\mathbf{r}_2) = \sum_{-L\le M'\le L} {\mathcal{D}^{L}_{MM'}}^{*}(\psi,\theta,\varphi)\,\Phi^{\pi}_{M'}(r_1,r_2,r_{12}) \tag{4}$$

where the $\mathcal{D}^{L}_{MM'}(\psi,\theta,\varphi)$ are the rigid top wave functions describing the rotation from the laboratory fixed coordinate system into a body fixed frame by the Euler angles ψ,θ,φ. Since the rigid top wave functions are known, the integration over the Euler angles can be carried out, leading to an effective Hamiltonian for each pair of good quantum numbers L and M containing Coriolis-like couplings of the $\Phi^{\pi}_{M'}(r_1,r_2,r_{12})$. To solve the remaining three-dimensional problem, we transform to perimetric coordinates [20,21]

$$\begin{aligned} x &= r_1 + r_2 - r_{12} \\ y &= r_1 - r_2 + r_{12} \qquad x,y,z \ge 0\,. \\ z &= -r_1 + r_2 + r_{12} \end{aligned} \tag{5}$$

As a basis set we chose products of Sturmian-type functions in the perimetric coordinates. The basis functions for the $L = 1$ case read

$$\Phi_{nkm}(r_1,r_2,r_{12}) = \phi_n(\alpha x)\phi_m(\beta y)\phi_k(\beta z) \tag{6}$$

where

$$\phi_n(u) = L_n(u)\,\mathrm{e}^{-u/2} \tag{7}$$

and $L_n(u)$ are the Laguerre polynomials. In the $L = 0$ case, $\mathcal{D}^{0}_{0\,0}(\psi,\theta,\varphi) = 1$ and we can incorporate the parity into the basis functions,

$$\begin{aligned} &\Phi^{\pi}_{nkm}(r_1,r_2,r_{12}) = \\ &\quad \phi_n(\alpha x)\big[\phi_m(\beta y)\phi_k(\beta z) + (-1)^{\pi}\phi_k(\beta y)\phi_m(\beta y)\big]\,, \end{aligned} \tag{8}$$

thus reducing the basis size since only states with $m \le k$ are needed. Although the usage of perimetric coordinates results in a rather complicated expression for the kinetic energy, it has several computational advantages. The volume element

$$\mathrm{d}V = \frac{8\pi^2}{32}(x+y)(x+z)(y+z)\,\mathrm{d}x\,\mathrm{d}y\,\mathrm{d}z \tag{9}$$

cancels all divergencies in the Hamiltonian when matrix elements are calculated. Since the perimetric coordinates all run independently from 0 to ∞, the three-dimensional integrals factorize into products of one-dimensional integrals. Finally, the orthogonality and recurrence relations of the Laguerre polynomials allow the matrix elements to be calculated analytically. Most of them vanish exactly, and by ordering the basis states in an appropriate way, a strongly banded Hamilton matrix can be achieved. In our calculations, we used $\alpha = 2\beta$ to get the correct asymptotic behaviour. We were able to use a maximum node number $\omega = 56$ in the $L = 1$ case and $\omega = 72$ in the $L = 0$ case leading to a basis size (band width) of 32 509 (2 898) and 34 447 (1 429), respectively, on a Fujitsu VX with 1 800 MByte memory.

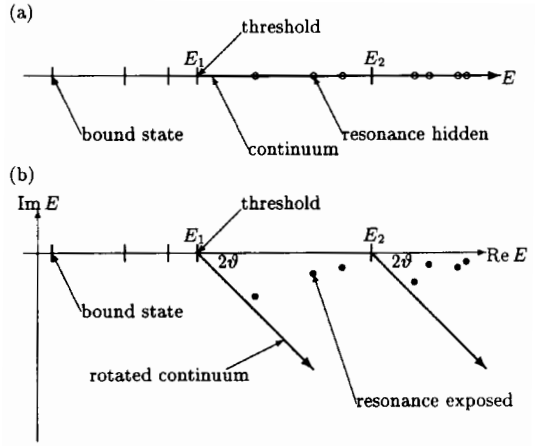

Fig. 1. (a) Schematic view of the spectrum of the three-body Coulomb system. The resonances are hidden in the continuum. (b) Schematic view of the spectrum of the complex scaled Hamiltonian. Whereas the bound states and thresholds remain at the same energies as in the unrotated case, the continua are rotated into the lower complex half plane by an angle 2ϑ. Resonances are exposed as complex poles $E_{\mathrm{res}} = E_{\mathrm{R}} - \mathrm{i}\Gamma/2$.

2.2 Complex scaling

To calculate the resonance parameters, we use the complex coordinate scaling [22–25] by formally writing

$$\beta = b\,\mathrm{e}^{\mathrm{i}\vartheta}\,. \tag{10}$$

In this approach, the radial part of the wave function is not complex conjugated when calculating matrix elements. Put in another way, for a resonant state which is described by a purely outgoing wave [26,27] the corresponding incoming wave is used as the adjoint state. This leads to the concept of bi-orthogonal sets [23,28,29]. The resonant state becomes square integrable and a norm can be defined. The corresponding scalar product, which we denote by $\langle\!\langle . | . \rangle\!\rangle$, is that of complex symmetric matrices. The complex rotated Hamiltonian $\mathcal{H}_\vartheta$ is thus no longer hermitian and can have complex eigenvalues (see Fig. 1).

In case of the mass polarisation, the interpretation of the complex expectation value $\langle\!\langle \mathbf{p}_1 \cdot \mathbf{p}_2 \rangle\!\rangle$ is straightforward since it is proportional to an energy shift. Its real part describes the shift of the resonance position

and its imaginary part the modification of the resonance width due to the motion of the nucleus. However, for other magnitudes as the interelectronic angle θ_{12}, the interpretation is somewhat more involved. Following a procedure from nuclear physics [30], we use the real part as the expectation value in the usual meaning,

$$\langle\, \mathcal{O} \,\rangle \equiv \mathrm{Re}\, \langle\!\langle \Psi_\vartheta |\, \mathcal{O}\, | \Psi_\vartheta \rangle\!\rangle \;, \tag{11}$$

where $\mathcal{O}$ is an operator an $|\Psi_\vartheta\rangle\!\rangle$ the state vector of the complex rotated wave function. The imaginary part then describes an additional contribution to the uncertainty of the expectation value which is due to the coupling of the resonance to the continuum [31].

We calculate several eigenvalues at a time by using a complex version of the Lanczos algorithm [32,33]. The eigenvalues are carefully checked for convergence by systematically increasing the basis size. The eigenvector and matrix elements are calculated using an inverse iteration algorithm. This program also optimizes β for each resonance separately such that

$$|\partial E_{\mathrm{res}}/\partial\beta| < \varepsilon \tag{12}$$

using the results from the Lanczos program as starting points. However, if the resonance obtained with the Lanczos algorithm is well converged with respect to the basis size, it fulfills the stability criterion (12) already in the first iteration which means that in these cases, E_{res} depends only weakly of the choice of b and ϑ.

3 Classification of doubly excited states

The doubly excited resonances are specified by their approximate group theoretical quantum numbers ${}_N(K,T)^A_n$ [34,35] and by the adiabatic molecular orbital quantum numbers in the parabolic limit $[N_1\, N_2\, m]^A_{\bar n}$ [36–38]. The latter are parabolic quantum numbers which describe the separated-atom (SA)[1] limit of the motion of the nucleus in the fields of the two electrons. Here, m is the projection of L onto the interelectronic axis and N_1 and N_2 are the number of parabolic nodes. A describes the symmetry with respect to the saddle $r_1 = r_2$ of the potential; states with $A = +1$ have an anti-node, states with $A = -1$ have a node on this saddle. The vibration-like quantum number $\bar n$ simply counts the states within the adiabatic potential. The group theoretical and molecular orbital (approximate) quantum numbers are connected as follows:

$$\begin{aligned} A &= A \qquad T = m \\ K &= N_2 - N_1 \\ N &= N_1 + N_2 + m + 1 \\ n &= \begin{cases} N + \bar n & \text{for } A = +1 \\ N + \bar n + 1 & \text{for } A = -1 \end{cases} . \end{aligned} \tag{13}$$

N is thus the principle quantum number of the residual hydrogen state when the outer electron is detached. However, n cannot be understood as a hydrogen-like principal quantum number since the outer electron is not bound in a Coulomb potential.

To assign the approximate quantum numbers we use the interelectronic angle since [34,39]

$$\langle \cos\theta_{12} \rangle \underset{n\to\infty}{\longrightarrow} -\frac{K}{N} \,. \tag{14}$$

A detailed discussion of the interelectronic angle and its connection to the approximate quantum numbers can be found in [39,40].

4 Results

We calculated the resonance position and width together with some expectation values for $H^-\ {}^1S^e$ states up to the $N = 10$ and for $H^-\ {}^1P^o$ states up to the $N = 8$ hydrogenic thresholds (-0.005 a.u. and -0.0078125 a.u., respectively). The resonance energies and widths are shown in Figure 2. The numbers can be found in Tables 3 and 4 in the Appendix. In addition, we give the expectation values for the cosine of the interelectronic angle as well as the mean radii $\langle r_< \rangle$ and $\langle r_> \rangle$ of the inner and the outer electron, respectively. The latter are obtained by reconstructing the unsymmetrized Lewis structure from the expectation values of the Jacobi coordinates $\mathbf{r} = (\mathbf{r}_1 + \mathbf{r}_2)/2$ and $\mathbf{r}_{12} = \mathbf{r}_2 - \mathbf{r}_1$ and the angle $\theta_{12} = \arccos\langle\cos\theta_{12}\rangle$ using triangle relations [31].

The states marked by crosses here are Feshbach-type resonances which bind to a hydrogenic parent state corresponding to the next higher threshold and form dipole series as predicted by [15]. Many of these resonances have been calculated before *e.g.* by adiabatic calculations in hyperspherical coordinates [10] and by complex scaling calculations in Hylleraas coordinates [11,12], though some of the $^1S^e$ resonances below the $N = 9$ threshold were originally assigned different quantum numbers.

Regarding Figure 2b, one can easily distinguish two classes of Feshbach-type $^1P^o$ resonances by their width. They differ in their approximate quantum number A. Since auto-detachment mainly goes via the saddle $r_1 = r_2$ of the potential, states with an anti-node there ($A = +1$) have a larger width than states with a node on this saddle ($A = -1$). In the case of $^1S^e$ resonances (Fig. 2a), there is only one such class since only states with $A = +1$ are allowed.

4.1 A new class of resonances?

The open symbols in Figure 2 mark complex poles which belong to another class. Only one of these (marked by the diamond) has been known before, it is the well-known $^1P^o$ ${}_N(K,T)^A_2 = {}_2(0,1)^+_2$ (or $[N_1\, N_2\, m]^A_{\bar n} = [0\,0\,1]^+_0$) shape resonance which has been studied for a long time. The other poles have not been discussed previously. Since those poles do not fit into the current understanding of the spectrum of H^-, the question arises whether they are physical solutions of the Schrödinger equation or numerical artefacts.

[1] This term comes from the corresponding H_2^+ molecule where the role of the protons and electrons is just reversed. Here, one should rather speak of separated electrons.

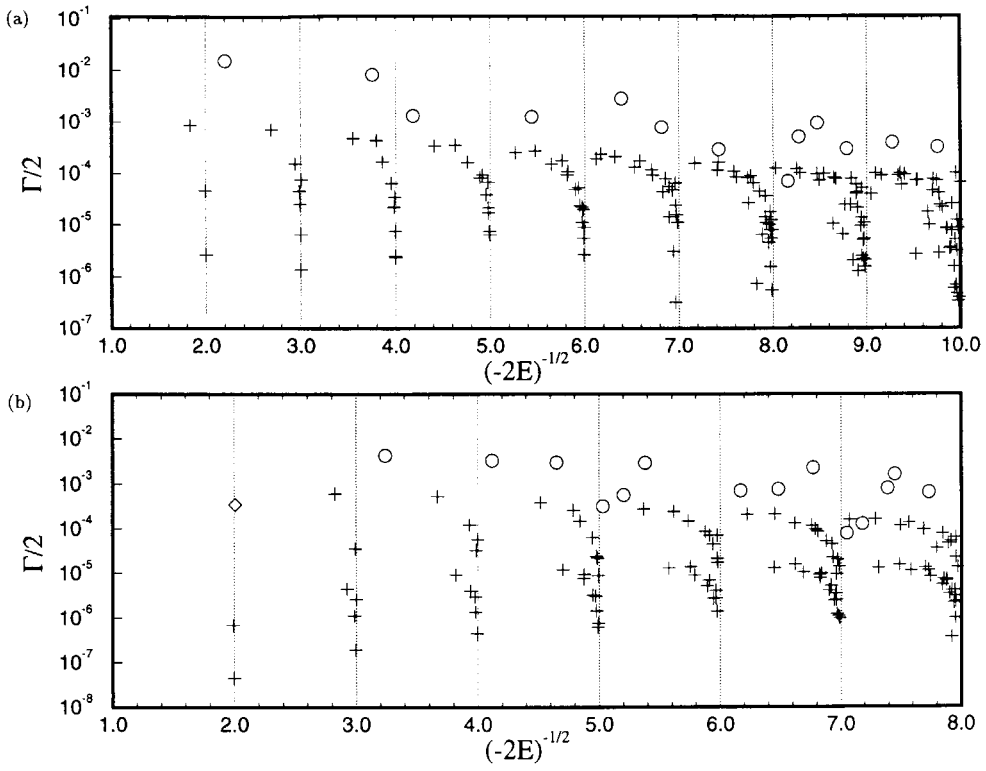

Fig. 2. Doubly excited resonances of H^- of $^1S^e$ symmetry (a) and $^1P^o$ symmetry (b). The open symbols mark shape resonances. The lowest $^1P^o$ shape resonance (marked by the diamond) has been known for a long time and can be described by a single adiabatic potential [10]. The others (marked by circles) are discussed here for the first time and are probably due to non-adiabatic couplings between those potentials.

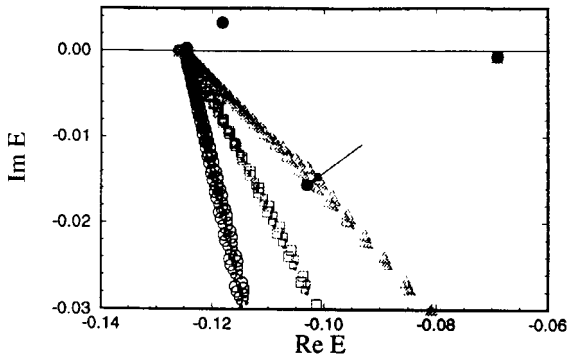

Fig. 3. Complex poles of $^1S^e$ symmetry in the vicinity of the $N = 2$ threshold. The results are shown for $\omega = 58$, 60, 62, and 64 (the smaller the symbol, the larger the basis set. The parameters were $\vartheta = 0.30$ (triangles), $\vartheta = 0.45$ (squares), and $\vartheta = 0.60$ (circles), $b = 0.33$ in all cases. For $\vartheta > 0.30$ an additional pole shows up as indicated by the arrow. It is rather well converged and present in all basis sets provided ϑ is large enough to uncover it. The other pole which shows up for $\vartheta = 0.60$ with a positive imaginary part, however, is a numerical artefact; it only shows up for this particular set of parameters and is badly converged (not visible on this scale).

4.1.1 Convergence

In Figure 3, we show our raw data for $^1S^e$ symmetry in the vicinity of the $N = 2$ threshold, calculated for three different rotation angles ϑ. For sufficiently large ϑ, an additional pole (indicated by the arrow) shows up, which is present in several basis sets employing various basis set parameters b and ϑ. It is very well converged with respect to the size of the basis set, as shown in Table 1. It even occurs in a numerically completely different calculation, which is shortly described in Section 4.3. Hence, from the computational point of view, we have no reason to dismiss this pole (and the other, similar ones) as unphysical. In each case, however, we made sure that these poles occur in several different basis sets and are well converged. (The pole situated closely above the threshold in Figure 3 which has the positive imaginary part is a numerical artefact. It occurs only for their specific parameter set and is only slightly converged.)

4.1.2 Properties

All these new resonances have the following properties:

1. they have a relative large width;
2. the expectation value of the cosine of the interelectronic angle, $\langle \cos \theta_{12} \rangle$, is very close to 0 and eventually positive;
3. the mean radius of the inner electron, $\langle r_< \rangle$, is small compared to that of the other states lying below the same hydrogenic threshold and compares rather well to those of the states below a lower threshold. A careful examination of $\langle r_< \rangle$ of some of the higher lying shape resonances suggests that they bind not to the next lower, but to even lower hydrogenic parent states;
4. the mass polarisation term is rather large.

From this, we conclude that the corresponding states are shape resonances binding to a lower N state of the hydrogenic parent atom. One of these shape resonances,

Table 1. The complex eigenvalue representing the $^1\mathrm{S}^\mathrm{e}$ shape resonance in H^- above the $N = 2$ threshold for increasing maximum node number ω of the basis set. The parameters for the basis set are (see Eq. (10)): $b = 0.33$ and $\vartheta = 0.45$.

ω	Re E	Im E
22	−0.103075569061	−0.015681789950
24	−0.103068260169	−0.015609087483
26	−0.103028806527	−0.015607083946
28	−0.103023163702	−0.015629114023
30	−0.103036538718	−0.015624912996
32	−0.103039992720	−0.015628075975
34	−0.103036538718	−0.015624912996
36	−0.103034378364	−0.015626571221
38	−0.103035117460	−0.015627989132
40	−0.103036012384	−0.015627703034
42	−0.103035936864	−0.015627157899
44	−0.103035614403	−0.015627146577
46	−0.103035574977	−0.015627331439
48	−0.103035677829	−0.015627373151
50	−0.103035712390	−0.015627317969
52	−0.103035684090	−0.015627292338
54	−0.103035666363	−0.015627306076
56	−0.103035672471	−0.015627317719
58	−0.103035679835	−0.015627315396
60	−0.103035679248	−0.015627310900
62	−0.103035676592	−0.015627310771
64	−0.103035676243	−0.015627312296

the $^1\mathrm{P}^\mathrm{o}$ ${}_N(K,T)_2^A = {}_2(0,1)_2^+$ (or $[N_1\,N_2\,m]_{\bar{n}}^A = [0\,0\,1]_0^+$) shape resonance, results in a very broad and prominent structure in the photo detachment cross-section and has been known for a long time. It is also present in adiabatic hyperspherical and earlier complex scaling calculation and results from a potential well in the $[N_1\,N_2\,m]^A = [0\,0\,1]^+$ adiabatic potential. Other adiabatic potentials with $K^A = 0^+$ (*e.g.* $^1\mathrm{S}^\mathrm{e}$ $[1\,1\,0]^+$, $^1\mathrm{S}^\mathrm{e}$ $[2\,2\,0]^+$, ... or $^1\mathrm{P}^\mathrm{o}$ $[1\,1\,1]^+$, $^1\mathrm{P}^\mathrm{o}$ $[2\,2\,1]^+$, ...) should also be able to hold resonances. Since the polarisability of the hydrogenic parent state increases with higher N, these states could lie below the corresponding dissociation threshold, as it is the case for the $^1\mathrm{S}^\mathrm{e}$ $[1\,1\,0]_0^+$, $^1\mathrm{S}^\mathrm{e}$ $[2\,2\,0]_0^+$, and $^1\mathrm{S}^\mathrm{e}$ $[3\,3\,0]_0^+$ below the $N = 3$, $N = 5$ and $N = 7$ thresholds or the $^1\mathrm{P}^\mathrm{o}$ $[1\,1\,1]_0^+$ and the $^1\mathrm{P}^\mathrm{o}$ $[2\,2\,1]_0^+$ states below the $N = 4$ and $N = 6$ thresholds, respectively. Eventually, some of these potentials could be deep enough to hold more then one resonance, and it could happen that the higher one were situated above the corresponding threshold, turning it into a shape resonance. Actually, we discovered two $^1\mathrm{S}^\mathrm{e}$ resonances with $K^A = 0^+$ binding with respect to the $N = 7$ state of H, but both lie below the corresponding threshold. Similarly, we found two $K^A = 0^+$ resonances below the $N = 9$ threshold.

There is evidence to believe that the discovered shape resonances are *not* of the type discussed above:

1. their expectation value of $\cos\theta_{12}$ does not match with that of $K^A = 0^+$ resonances below the corresponding threshold;
2. their mean radii $\langle r_< \rangle$ and $\langle r_> \rangle$ are smaller than those of the $K^A = 0^+$ resonances mentioned above. If both the $K^A = 0^+$ and the shape resonances would reside in the same potential, the expectation values for the shape resonance should be larger;
3. some of these resonances lie rather highly above the next lower threshold that would support $K^A = 0^+$ states. The adiabatic potentials of $^1\mathrm{P}^\mathrm{o}$ symmetry calculated in hyperspherical coordinates [10] would not support the resonances presented here;
4. there should not be any resonances with $K^A = 0^+$ above thresholds with even N in $^1\mathrm{S}^\mathrm{e}$ symmetry and odd N in $^1\mathrm{P}^\mathrm{o}$ symmetry. However, we find shape resonances even there. (The $K^A = 0^-$ potentials calculated for $^1\mathrm{P}^\mathrm{o}$ symmetry [10] are purely repulsive and should not support shape resonances. Such potentials do not exist in $^1\mathrm{S}^\mathrm{e}$, where only $A = +1$ is allowed.)

We hence believe that these new shape resonances are due to a non-adiabatic coupling between different binding and anti-binding adiabatic potentials which corresponds to a mixing of ${}_N(K,T)$ or $[N_1\,N_2\,m]$ approximate quantum numbers where both positive and negative K would occur. This is the reason why we did not even try to assign approximate quantum numbers to these states.

4.2 Variation of the nuclear charge

The approximate character of the two-electron quantum numbers has been known since a long time [35] and was recently studied in detail by investigating the interelectronic angle in $^1\mathrm{S}^\mathrm{e}$ states of helium [39,40]. It was found that for $N \geq 3$, the $[N_1\,N_2\,m]^A = [0\;N{-}1\;0]^+$ and $[1\;N{-}2\;0]^+$ adiabatic basis states mix in avoided crossings of the resonance energies under a variation of the nuclear charge Z. As N increases, more and more of these adiabatic basis states are involved. At $N = 10$, only the $[9\,0\,0]^+$ series can be described as pure. As Z approaches one, the number of avoided crossings increases and hence does the mixing of adiabatic basis states. We believe that it is by this mixing that shape resonances with $\langle\cos\theta_{12}\rangle > 0$ can occur in H^- although the adiabatic potentials with $K < 0$ are purely repulsive.

In Figure 4, we show the variation of the lowest doubly excited $^1\mathrm{S}^\mathrm{e}$ energy levels with the nuclear charge Z, which corresponds to a variation of the relative strength of the electron-electron interaction. At the left margin, we have the case of uncorellated electrons which can be described as a product state of hydrogenic wave functions. Moving to the right, the electron-electron correlation increases, but the states are still well described by the approximate ${}_N(K,T)_n^A$ or $[N_1\,N_2\,m]_{\bar{n}}^A$ quantum numbers until the energy levels undergo avoided crossings where they exchange character. This would lead to a mixing of (adiabatic) basis states carrying the approximate quantum numbers. Eventually, a continuum state residing in an anti-binding adiabatic potential with $\langle\cos\theta_{12}\rangle > 0$ could acquire sufficient bound state character to prevail as a short-lived shape resonance as it is shown here for the lowest $^1\mathrm{S}^\mathrm{e}$ shape resonance marked by the arrow on the right margin.

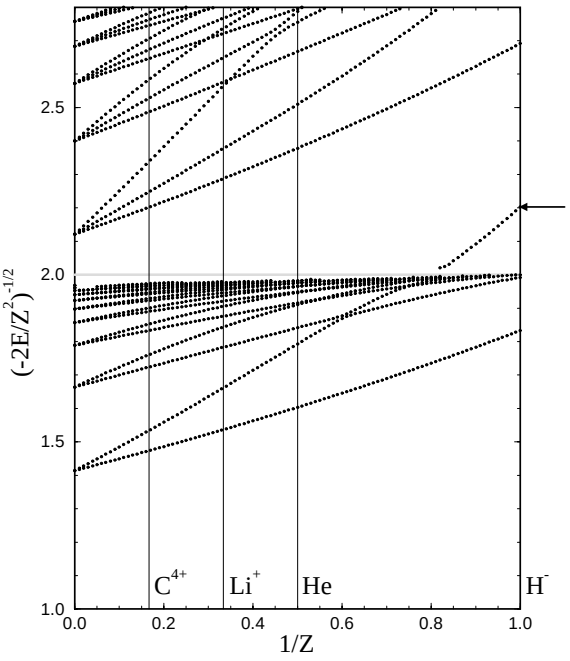

Fig. 4. Resonance energies of $^1\mathrm{S}^\mathrm{e}$ symmetry under variation of the relative strength of the electron-electron interaction. The approximate quantum numbers are mixed in avoided crossings between the energy levels. The arrow marks the position of the lowest $^1\mathrm{S}^\mathrm{e}$ shape resonance which evolves from the $N = 2$ manifold. In the threshold region (marked by the horizontal line), accurate results cannot be obtained since we have to truncate our basis set (in this calculation, it was truncated at $\omega = 52$).

Why have these resonances not been known previously? On the theoretical side, they do not occur in adiabatic hyperspherical calculations. This is consistent with the idea that the exist due to a non-adiabatic coupling of MO (or other) adiabatic basis states. Further, since these resonances are rather broad and situated quite closely above the corresponding thresholds, they require a rather large angle ϑ to be uncovered in complex scaling calculations (see also [45]).

4.3 Photo-absorption cross-section

To investigate whether these resonances should be detectable in an experiment, we calculate the photo-absorption cross-section which is given by

$$\sigma(\omega) = \frac{4\pi}{3}\frac{\omega}{c}\,\mathrm{Im}\left(\sum_n \frac{\langle\langle \Psi_0^\vartheta |\, d\, | \Psi_n^\vartheta \rangle\rangle^2}{E_n - E_0 - \hbar\omega}\right) . \qquad (15)$$

Here, d is the operator for an optical dipole transition, E_0 is the energy and Ψ_0^ϑ the (complex rotated) wave function of the ground state, respectively. The sum runs over all poles of the complex rotated Hamiltonian, *i.e.* over both resonances and continuum states [14]. Here, we use d in its length form, $d = (\mathbf{r}_1 + \mathbf{r}_2)\hat{\boldsymbol{\epsilon}}$, where $\hat{\boldsymbol{\epsilon}}$ is the polarisation vector of the light source. The calculations are performed for unpolarized light.

Unfortunately, the cross-section calculated in our Sturmian basis set is less accurate than the resonance position and width or other expectation values. For reasons of numerical stability, we are forced to use the same β for the calculation of *all* states occurring in (15) including the ground state. To achieve good convergence for the resonant states, we use $b \leq 1/N$ for states below the Nth threshold. Thus for highly excited states, the calculation of the photo-absorption cross-section is actually hampered by a less accurate presentation of the ground state.

We therefore use a different numerical scheme to calculate the photo-absorption cross-section which based on complex scaling and B-spline basis functions. This approach treats both ground state an resonant state basis functions on equal footing. It is described in detail in [14,46].

Photo excitation goes preferably to ${}_N(K,T)^A_n = {}_N(N-2,1)^+_n$ states ($[N_1\, N_2\, m]^A = [0\, N-2\, 1]^+$ in MO notation) [37]. This is the reason why the $^1\mathrm{P}^\mathrm{o}$ ${}_2(0,1)^+_2$ shape resonance just above the $\mathrm{H}(N = 2)$ threshold is so strong. The other shape resonances do not belong to this class and hence will be rather weak. This is demonstrated in Figure 5 where we show the photo-absorption cross-section from the ground state in the energy region between the $N = 3$ and $N = 4$ hydrogenic thresholds where the next higher $^1\mathrm{P}^\mathrm{o}$ shape resonance is situated. The cross-section is calculated using (15) (full line). For comparison, the dashed line shows the cross-section without the presence of the shape resonance, *i.e.* where this eigenvalue is omitted in the summation in (15). The position and width of the shape resonance is also marked. Clearly, its presence leads to broad but weak modulation of the "background" in between the sharp Feshbach-like peaks which makes it hard to detect experimentally.

However, remanents of one such shape resonances might have already been seen in an experiment. Harris *et al.* [4,5] reported a shallow dip just above the $N = 4$ hydrogenic threshold at a photon energy of 13.55 eV. This coincides with the position of the $^1\mathrm{P}^\mathrm{o}$ shape resonance we found at $E_\mathrm{res} = (-0.02950891 - \mathrm{i}\,0.00329825)\,\mathrm{a.u.}$ However, its FWHM would be $\Gamma = 0.17940\,\mathrm{eV}$, which is much broader than the observed dip. This resonance would strongly overlap with the threshold itself. The consequences of this are not fully understood yet and need further investigation. Unfortunately, we have not succeeded in getting converged results for the photo-absorption cross-section with either approach since one needs a rather large angle ϑ to uncover the shape resonance.

There is another conceptual problem with these resonances. In a very crude classical model, we take the surplus energy of the resonance above the threshold as the kinetic energy of its outer electron, $E_\mathrm{kin} = E_\mathrm{R} - E_\mathrm{thr}$, to calculate the distance that it travels under the lifetime $\tau = 1/\Gamma$ of the doubly excited state. For the resonance above,

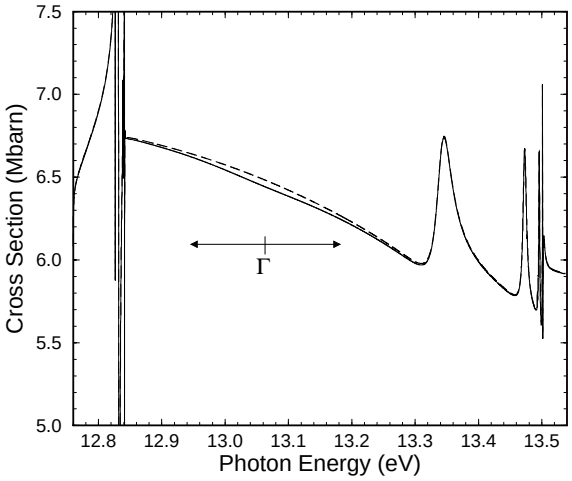

Fig. 5. Photo detachment cross-section for H^- between the $N = 3$ and $N = 4$ thresholds. The full line is the total cross-section including the $^1P^o$ shape resonance at $E = -0.04767516$ a.u., the dashed line shows the cross-section without this resonance. Both the resonance position and full width at half maximum are marked. The shape resonance gives rise to a weak and broad structure in the "background" which is hard to detect.

this model implies that the outer electron would travel only on a 15° arc of a circular orbit with of radius $\langle r_> \rangle$. On the other hand, the same estimate leads to a 245° arc for the well-known $^1P^o$ resonance just above the $N = 2$ threshold. Of course the question arises whether such a state still can be called a resonance. A similar situation is found in the recently published contribution on the question whether there exist resonances in H^{2-} [47]. The resonances proposed there are also not present in adiabatic calculations [48,49].

4.4 Mass polarisation

In Tables 3 and 4 in the Appendix, we also show our results for the mass polarisation term. For $^1S^e$ states, $\langle\langle \mathbf{p}_1 \cdot \mathbf{p}_2 \rangle\rangle$ is calculated as expectation value from the resonance wave function for $M \to \infty$, while for $^1P^o$ states, we calculate both $E_{\rm res}^{\infty}$ and $E_{\rm res}^{\rm M}$ by the Lanczos algorithm to determine $\langle\langle \mathbf{p}_1 \cdot \mathbf{p}_2 \rangle\rangle$ according to (2) and (3).

As was suggested in [18], the mass polarisation contribution within a dipole series characterized by common $[N_1\, N_2\, m]^A$ or ${}_N(K,T)^A$ approximate quantum numbers decreases when approaching the threshold. However, this decrease is not necessarily monotonic. It seems that the larger N_2, the more zeroes can both real and imaginary part of $\langle\langle \mathbf{p}_1 \cdot \mathbf{p}_2 \rangle\rangle$ have. Further, it was suggested that the specific shift of the resonance energies given by $\mathrm{Re}\,\langle\langle \mathbf{p}_1 \cdot \mathbf{p}_2 \rangle\rangle$ should be larger for states with $A = +1$ than for states with $A = -1$ [18]. This is not found in our calculations. However, we find that $\mathrm{Im}\,\langle\langle \mathbf{p}_1 \cdot \mathbf{p}_2 \rangle\rangle$, *i.e.* the variation of the width, is about one order of magnitude larger for $A = +1$ states than for $A = -1$ states. Looking at table 4 one finds, that $\mathrm{Im}\,\langle\langle \mathbf{p}_1 \cdot \mathbf{p}_2 \rangle\rangle$ is of the order of 10^{-5} for $A = -1$ states, but of the order of 10^{-4} for $A = +1$ states. On the other hand, these states also have a larger width, so that the relative change of the lifetime is approximately the same. The shape resonances, however, have comparably large mass polarisation contributions. But even here, the shift of the resonance energy and the variation of their width is small when compared to their total width Γ.

Table 2. Mass polarisation contributions for some resonant states with higher L.

	$E_{\rm R}$	$\Gamma/2$	$\mathrm{Re}\langle\langle \mathbf{p}_1 \cdot \mathbf{p}_2 \rangle\rangle$	$\mathrm{Im}\langle\langle \mathbf{p}_1 \cdot \mathbf{p}_2 \rangle\rangle$
$^1D^e$	−0.12792	0.00015	−0.0063	−0.0005
	−0.06595	0.00083	0.0014	0.0017
$^1F^o$	−0.05514	0.00041	−0.0012	0.0010
$^3F^o$	−0.05544	0.00013	0.0001	0.0001

One might of course ask whether other symmetries could have much larger mass polarisation terms. We have thus tested a few other symmetries using the method described in [14]. The results are given in Table 2. The positions and widths of these resonances agree well with earlier calculations [50,51]. The mass polarisation contributions for these states are found to be of the same order of magnitude as for the $^1S^e$ and $^1P^o$ symmetry. Rislove *et al.* [19] measured a specific mass shift of the $^1D^e$ resonance below the $N = 2$ threshold of (-2.4 ± 1.1) meV corresponding to $\mathrm{Re}\,\langle\langle \mathbf{p}_1 \cdot \mathbf{p}_2 \rangle\rangle = (-0.16 \pm 0.07)$ a.u. which is in clear disagreement with our calculation. However, our calculation is in good agreement with other calculations cited in [19].

The mass polarisation term $\langle\langle \mathbf{p}_1 \cdot \mathbf{p}_2 \rangle\rangle$ is often discussed in connection with the search for correlation in the electron momenta. This connection is suggested by its similarity to $\langle\langle \cos\theta_{12} \rangle\rangle = \langle\langle (\mathbf{r}_1 \cdot \mathbf{r}_2)/(r_1 r_2) \rangle\rangle$ which in turn is connected to the K approximate quantum number expressing angular correlation. However, the analysis of $\langle\langle \mathbf{p}_1 \cdot \mathbf{p}_2 \rangle\rangle$ is more complicated since it not only contains the angle between the electron's momenta, but also their size. Hence, we are afraid that studying the mass polarisation term will not lead to an understanding of electron momentum correlation. Our results do not suggest any simple relation similar to (14). Moreover, the effects of the mass polarisation to the resonance energies are suppressed by the relative large mass of the nucleus. For a much lighter system like Ps^-, momentum correlation should be more pronounced.

5 Conclusion

We presented a detailed study of doubly excited resonances in the negative hydrogen ion of both $^1S^e$ and $^1P^o$ symmetry using complex coordinate scaling in a Sturmian-type basis set in perimetric coordinates. The results are given in the appendix for further reference. We list the resonance energies and widths together with some characteristic expectation values, including mass polarisation.

Energies and widths of approximately half of the states have been published earlier [11,12,52], but are included in the table for convenience. Here, we give our own results where we were able to press convergence even further. The energies and widths of the highly lying, asymmetrically excited states and all the expectation values are published here for the first time.

We also found a new type of shape resonances which have not been known previously. We suggest that they are due to couplings between various adiabatic potentials and hence a mixing of approximate quantum numbers which would prevent them from occurring in adiabatic calculations. They result in broad and weak structures in the photo absorption cross-section which are hard to distinguish from the smooth "background" coming from non-resonant photo detachment, but with improved statistics it is maybe possible to investigate them experimentally. One of these shape resonances, the lowest $^1\mathrm{P^o}$ shape resonance above the $N = 4$ hydrogenic threshold, coincides in its position with a hitherto unexplained structure in the photo-detachment cross-section at a photon energy of 13.55 eV [4,5]. Unfortunately, we did not succeed in obtaining converged results for the cross-section that would include this shape resonance. A verification of the shape resonances is thus still an open question.

We like to thank Jan-Michael Rost for fruitful discussions. This work was carried out under the European Union's TMR Programme contract no ERBFMBICT961473. Computation time at the Center of Parallel Computing (PDC) is gratefully acknowledged.

References

1. M.E. Hamm, R.W. Hamm, J. Donahue, P.A.M. Gram, J.C. Pratt, M.A. Yates, R.D. Bolton, D.A. Clark, H.C. Bryant, C.A. Frost, W.W. Smith, Phys. Rev. Lett. **43**, 1715 (1979).
2. D.W. MacArthur, K.B. Butterfield, D.A. Clark, J.B. Donahue, P.A.M. Gram, H.C. Bryant, C.J. Harvey, W.W. Smith, G. Comtet, Phys. Rev. A **32**, 1921 (1985).
3. S. Cohen, H.C. Bryant, C.J. Harvey, J.E. Stewart, K.B. Butterfield, D.A. Clark, J.B. Donahue, D.W. MacArthur, G. Comtet, W.W. Smith, Phys. Rev. A **36**, 4728 (1987).
4. P.G. Harris, H.C. Bryant, A.H. Mohagheghi, R.A. Reeder, H. Sharifian, C.Y. Tang, H. Tootoonchi, J.B. Donahue, C.R. Quick, D.C. Rislove, W.W. Smith, J.E. Stewart, Phys. Rev. Lett. **65**, 309 (1990).
5. P.G. Harris, H.C. Bryant, A.H. Mohagheghi, R.A. Reeder, C.Y. Tang, J.B. Donahue, C.R. Quick, Phys. Rev. A **42**, 6443 (1990).
6. M. Halka, E.P. Mackerrow, W. Miller, A.H. Mohagheghi, C.Y. Tang, S. Cohen, J.B. Donahue, A. Hsu, C.R. Quick, J. Tiee, K. Rosza, Phys. Rev. A **44**, 6127 (1991).
7. P. Balling, P. Kristensen, H.H. Andersen, U.V. Pedersen V.V. Petrunin, L. Præstgaard, H.K. Haugen, T. Andersen, Phys. Rev. Lett. **77**, 2905 (1996).
8. J.T. Broad, W.P. Reinhardt, Phys. Rev. A **14**, 2159 (1976).
9. N. Koyama, A. Takafuji, M. Matsuzawa, J. Phys. B: At. Mol. Opt. Phys. **22**, 553 (1989).
10. H.R. Sadeghpour, C.H. Greene, Phys. Rev. Lett. **65**, 313 (1909).
11. Y.K. Ho, J. Phys. B: At. Mol. Opt. Phys. **23**, L71 (1990).
12. Y.K. Ho, Phys. Rev. A **45**, 148 (1992).
13. J. Tang *et al.*, Phys. Rev. A **49**, 1021 (1994).
14. E. Lindroth, Phys. Rev. A **52**, 2737 (1995).
15. M. Gailitis, R. Damburg, Proc. Phys. Soc. Lond. A **82**, 192 (1963).
16. T. Purr, H. Friedrich, A.T. Stelbovics, Phys. Rev. A **57**, 308 (1998).
17. E. Lindroth, A. Bürgers, N. Brandefelt, Phys. Rev. A **57**, R685 (1998).
18. H.H. Andersen, P. Balling, P. Kristensen, U.V. Pedersen, S.A. Aseyev, V.V. Petrunin, T. Andersen, Phys. Rev. Lett. **79**, 4770 (1997).
19. D.C. Rislove, C.E.M. Strauss, H.C. Bryant, M.S. Gulley, D.J. Funk, X.M. Zhao, W.A. Miller, Phys. Rev. A **58**, 1889 (1998) 1889; Phys. Rev. A **59**, 906 (1999).
20. A.S. Coolidge, H.M. James, Phys. Rev. **12**, 518 (1937).
21. C.L. Pekeris, Phys. Rev. **112**, 1649 (1958).
22. E. Balslev, J.M. Combes, Comm. Math. Phys. **22**, 280 (1971).
23. B.R. Junker, Adv. At. Mol. Phys. **18**, 207 (1982).
24. Y.K. Ho, Phys. Rep. **99**, 1 (1983).
25. A. Buchleitner, B. Grémaud, D. Delande, J. Phys. B: At. Mol. Opt. Phys. **27**, 2663 (1994).
26. G. Gamow, Z. Phys. **51**, 204 (1928).
27. A.J.F. Siegert, Phys. Rev. **56**, 750 (1939).
28. P.M. Morse, H. Feshbach, *Methods of Theoretical Physics* (McGraw-Hill, New York, 1958), Vol. I.
29. N. Hokkyo, Prog. Theor. Phys. **33**, 1116 (1964).
30. T. Berggren, Nucl. Phys. A **109**, 365 (1968).
31. A.Bürgers, J.M. Rost, J. Phys. B: At. Mol. Opt. Phys. **29**, 3825 (1996).
32. T. Ericsson, A. Ruhe, Math. Comp. **35**, 1251 (1980).
33. D. Wintgen, D. Delande, J. Phys. B: At. Mol. Opt. Phys. **26**, L399 (1993).
34. D.R. Herrick, O. Sinanoğlu, Phys. Rev. A **11**, 97 (1975).
35. D.R. Herrick, Adv. Chem. Phys. **52**, 1 (1983).
36. J.M. Feagin, J.S. Briggs, Phys. Rev. Lett. **57**, 984 (1986); Phys. Rev. A **37**, 4599 (1988).
37. J.M. Rost, J.S. Briggs, J. Phys. B: At. Mol. Opt. Phys. **24**, 4293 (1991).
38. J.M. Rost, K. Schulz, M. Domke, G. Kaindl, J. Phys. B: At. Mol. Opt. Phys. **30**, 4663 (1997).
39. A. Bürgers, N. Brandefelt, E. Lindroth, J. Phys. B: At. Mol. Opt. Phys. **31**, 3181 (1998).
40. A. Bürgers J. Phys. B: At. Mol. Opt. Phys. **32**, 845 (1999).
41. D. Wintgen, H. Friedrich, Phys. Rev. A **35**, 1628 (1987).
42. A. Bürgers, D. Wintgen, J.M. Rost, J. Phys. B: At. Mol. Opt. Phys. **28**, 3163 (1995).
43. A. Bürgers, H. Bachau, J. Phys. B: At. Mol. Opt. Phys. **30**, 4163 (1997).
44. A. Pathak, P.G. Burke, K.A. Berrington, J. Phys. B: At. Mol. Opt. Phys. **22**, 2759 (1989).
45. Y.K. Ho, Phys. Rev. A **49**, 3659 (1994).
46. N. Brandefelt, E. Lindroth, Phys. Rev. A **59**, 2691 (1999).
47. M. Bylicki, C.A. Nicolaides, J. Phys. B: At. Mol. Opt. Phys. **31**, L685 (1998).
48. C.D. Lin, Chin. J. Phys. **35**, 462 (1997).
49. T. Moroshita, C.D. Lin, C.G. Bao, Phys. Rev. Lett. **80**, 464 (1998).
50. A.K. Bhatia, Y.K. Ho, Phys. Rev. A **41**, 504 (1990).
51. Y.K. Ho, Phys. Lett. A **189**, 3874 (1994).
52. M.Chen, J. Phys. B **30**, 1669 (1997).

Appendix: Tables

Table 3. Non-relativistic resonance energies and width (calculated for infinite nuclear mass), interelectronic angle, the mean radii for the inner and outer electron and the mass polarisation for the $^1S^e$ states of H^-. The states are identified by their group theoretical quantum numbers ${}_N(K,T)^A_n$ and parabolic molecular orbital quantum numbers $[N_1\,N_2\,m]^A_{\tilde{n}}$. The results are given in atomic units ($e = m_e = \hbar = 4\pi\varepsilon_0 = 1$) and are converged to all digits shown.

state		E_R	$\Gamma/2$	$\langle\cos\theta_{12}\rangle$	$\langle r_<\rangle$	$\langle r_>\rangle$	$\mathrm{Re}\langle\langle \mathbf{p}_1\cdot\mathbf{p}_2\rangle\rangle$	$\mathrm{Im}\langle\langle \mathbf{p}_1\cdot\mathbf{p}_2\rangle\rangle$
${}_1(0,0)^+_1$	$[0\,0\,0]^+_0$	−0.52775101654	—	−0.105148	1.7102	3.7102	0.032879782	—
${}_2(1,0)^+_2$	$[0\,1\,0]^+_0$	−0.14877625394	0.00086661817	−0.506000	4.7693	10.3699	0.000964503	0.001412238
${}_2(1,0)^+_3$	$[0\,1\,0]^+_1$	−0.12602006374	0.00004526486	−0.499773	5.1247	40.2588	0.000045151	0.000047937
${}_2(1,0)^+_4$	$[0\,1\,0]^+_2$	−0.12505785	0.00000261	−0.493217	5.3	168.7	0.000002	0.000003
shape		−0.103035676	0.015627312	0.123496	5.7929	8.7209	0.0165390	−0.0259438
${}_3(2,0)^+_3$	$[0\,2\,0]^+_0$	−0.06900579528	0.00070944235	−0.646297	10.2203	22.3287	0.000707031	0.002644300
${}_3(2,0)^+_4$	$[0\,2\,0]^+_1$	−0.05778163192	0.00015416915	−0.660131	11.1997	46.9345	−0.000303307	0.000487553
${}_3(2,0)^+_5$	$[0\,2\,0]^+_2$	−0.05600661052	0.00002515647	−0.643028	10.9803	102.1046	−0.000020377	0.000214531
${}_3(2,0)^+_6$	$[0\,2\,0]^+_3$	−0.0556491427	0.0000065009	−0.659062	11.04	230.36	−0.00001733	0.00001894
${}_3(2,0)^+_7$	$[0\,2\,0]^+_4$	−0.05557495	0.00000138	−0.65934	15.	505.	−0.0000038	0.0000038
${}_3(0,0)^+_3$	$[1\,1\,0]^+_0$	−0.05614328476	0.00004483091	−0.132554	11.3985	30.4209	0.003426781	0.000219548
shape		−0.03543901515	0.00813107640	−0.016653	14.2332	18.9336	0.020531353	−0.013023061
${}_4(3,0)^+_4$	$[0\,3\,0]^+_0$	−0.03963554677	0.00047708478	−0.724761	17.2497	39.7209	0.000731177	0.001909780
${}_4(3,0)^+_5$	$[0\,3\,0]^+_1$	−0.03356680740	0.00017022027	−0.739368	18.9159	65.6714	−0.000428359	0.000553021
${}_4(3,0)^+_6$	$[0\,3\,0]^+_2$	−0.03201748612	0.00006393837	−0.741525	19.3088	112.4864	−0.000181455	0.000227401
${}_4(3,0)^+_7$	$[0\,3\,0]^+_3$	−0.03150704045	0.00002255121	−0.739348	19.1077	195.1177	−0.000055765	0.000089601
${}_4(3,0)^+_8$	$[0\,3\,0]^+_4$	−0.03133587618	0.00000751284	−0.742733	19.210	341.524	−0.00002149	0.00002832
${}_4(3,0)^+_9$	$[0\,3\,0]^+_5$	−0.03127883	0.00000252	−0.74256	20.	596.	−0.0000075	0.0000097
${}_4(1,0)^+_4$	$[1\,2\,0]^+_0$	−0.03472003578	0.00043288174	−0.293308	19.4933	38.5300	0.001323821	−0.000081085
${}_4(1,0)^+_5$	$[1\,2\,0]^+_1$	−0.03146854508	0.00003478236	−0.269247	19.7857	104.9574	0.000272350	0.000019316
${}_4(1,0)^+_6$	$[1\,2\,0]^+_2$	−0.031263875	0.000002377	−0.247255	19.72	367.88	0.00002116	0.00000293
shape		−0.0285503068	0.0013187669	−0.002742	22.7511	35.4331	0.003069312	−0.002298963
${}_5(4,0)^+_5$	$[0\,4\,0]^+_0$	−0.02570040545	0.00034468519	−0.775320	26.2938	62.0818	0.000810221	0.001409505
${}_5(4,0)^+_6$	$[0\,4\,0]^+_1$	−0.02207410441	0.00016640612	−0.787234	29.3032	90.1167	−0.000335607	0.000617013
${}_5(4,0)^+_7$	$[0\,4\,0]^+_2$	−0.02089098994	0.00008477270	−0.790071	29.9227	133.9052	−0.000194904	0.000376560
${}_5(4,0)^+_8$	$[0\,4\,0]^+_3$	−0.02038700741	0.00003885873	−0.792230	29.7187	204.1983	−0.000075029	0.000193832
${}_5(4,0)^+_9$	$[0\,4\,0]^+_4$	−0.0201680756	0.0000173403	−0.817482	29.5572	319.7972	−0.000035556	0.000099111
${}_5(4,0)^+_{10}$	$[0\,4\,0]^+_5$	−0.020072765	0.000007454	−0.793538	29.591	479.577	−0.00001006	0.00004036
${}_5(2,0)^+_5$	$[1\,3\,0]^+_0$	−0.02331649404	0.00035444723	−0.403242	29.6671	58.8784	0.001085553	0.000564679
${}_5(2,0)^+_6$	$[1\,3\,0]^+_1$	−0.02068526640	0.00009568618	−0.410881	30.6884	105.5668	0.000237351	0.000187365
${}_5(2,0)^+_7$	$[1\,3\,0]^+_2$	−0.02016826882	0.00002179667	−0.357822	30.1202	186.4042	0.000134863	0.000073275
${}_5(2,0)^+_8$	$[1\,3\,0]^+_3$	−0.02004207571	0.00000647135	−0.393123	30.255	394.705	0.00001704	0.00001237
${}_5(0,0)^+_5$	$[2\,2\,0]^+_0$	−0.02021030174	0.00006895984	−0.143592	32.4781	72.7392	0.001444318	0.000328415
shape		−0.01688487596	0.00126851629	0.004229	37.2919	51.2972	0.004254580	−0.000400141
shape		−0.01588872720	0.00439433907	−0.113195	28.1186	36.5683	0.016717692	−0.009183702
${}_6(5,0)^+_6$	$[0\,5\,0]^+_0$	−0.0180119076	0.0002554607	−0.810550	36.9331	89.6948	0.000785213	0.000982209
${}_6(5,0)^+_7$	$[0\,5\,0]^+_1$	−0.01567107356	0.00015176084	−0.819559	41.5889	119.9481	−0.000214044	0.000582548
${}_6(5,0)^+_8$	$[0\,5\,0]^+_2$	−0.01479483303	0.00009476959	−0.825404	42.9590	161.5933	−0.000107464	0.000494645
${}_6(5,0)^+_9$	$[0\,5\,0]^+_3$	−0.01435896271	0.00004941459	−0.825674	42.3685	223.3434	0.000045857	0.000295288
${}_6(5,0)^+_{10}$	$[0\,5\,0]^+_4$	−0.01413199457	0.00002385068	−0.826597	42.2996	313.4730	0.000073744	0.000143824
${}_6(5,0)^+_{11}$	$[0\,5\,0]^+_5$	−0.0140136232	0.0000113388	−0.825008	42.610	442.380	0.00005352	0.00006463
${}_6(5,0)^+_{12}$	$[0\,5\,0]^+_6$	−0.01395254	0.00000551	−0.827768	41.9	627.0	0.0000312	0.0000306
${}_6(3,0)^+_6$	$[1\,4\,0]^+_0$	−0.0166695354	0.0002790225	−0.484815	40.2767	86.2203	0.000624644	0.000394056
${}_6(3,0)^+_7$	$[1\,4\,0]^+_1$	−0.01475610758	0.00011071232	−0.492618	42.1209	129.5636	0.000123554	0.000084723
${}_6(3,0)^+_8$	$[1\,4\,0]^+_2$	−0.01421467987	0.00005304750	−0.495280	43.2860	201.3953	0.000041530	0.000070311
${}_6(3,0)^+_9$	$[1\,4\,0]^+_3$	−0.01401288263	0.00002257653	−0.491350	42.8398	319.6700	0.000021548	0.000036273
${}_6(3,0)^+_{10}$	$[1\,4\,0]^+_4$	−0.013935268	0.000008969	−0.48833	42.937	520.749	0.00000443	0.00001494

Table 3. *Continued.*

state		E_{R}	$\Gamma/2$	$\langle\cos\theta_{12}\rangle$	$\langle r_<\rangle$	$\langle r_>\rangle$	$\mathrm{Re}\langle\langle \mathbf{p}_1\cdot\mathbf{p}_2\rangle\rangle$	$\mathrm{Im}\langle\langle \mathbf{p}_1\cdot\mathbf{p}_2\rangle\rangle$
${}_6(1,0)^+_6$	$[2\,3\,0]^+_0$	−0.01505883976	0.00017964991	−0.238806	45.4366	83.2309	0.000678739	−0.000132489
${}_6(1,0)^+_7$	$[2\,3\,0]^+_1$	−0.01396761795	0.00002029182	−0.207821	44.673	189.812	0.00021838	0.00002492
shape		−0.0131288011	0.0002400331	−0.033856	51.462	83.774	0.001381109	−0.000482012
shape		−0.012239305	0.002846921	0.19467	45.519	77.107	0.0005262	−0.0029562
${}_7(6,0)^+_7$	$[0\,6\,0]^+_0$	−0.013323093	0.000193673	−0.836171	49.2587	122.5013	0.00067732	0.00068849
${}_7(6,0)^+_8$	$[0\,6\,0]^+_1$	−0.01172242713	0.00013425005	−0.843091	55.6410	155.0580	−0.000132233	0.000506431
${}_7(6,0)^+_9$	$[0\,6\,0]^+_2$	−0.01107655511	0.00009344814	−0.845252	54.9763	195.6101	0.000041769	0.000496261
${}_7(6,0)^+_{10}$	$[0\,6\,0]^+_3$	−0.01072165030	0.00004467633	−0.850111	56.9697	249.4060	0.000238379	0.000222573
${}_7(6,0)^+_{11}$	$[0\,6\,0]^+_4$	−0.01050922393	0.00001456737	−0.850774	57.1039	324.5148	0.000193499	0.000032149
${}_7(6,0)^+_{12}$	$[0\,6\,0]^+_5$	−0.01038320642	0.00000306967	−0.850529	57.3045	422.4547	0.000120172	−0.000006755
${}_7(6,0)^+_{13}$	$[0\,6\,0]^+_6$	−0.0103087999	0.0000003276	−0.851034	57.200	557.352	0.000066315	−0.000002211
${}_7(6,0)^+_{14}$	$[0\,6\,0]^+_7$	−0.01026473	0.00000009	−0.852061	56.91	745.67	0.0000331	0.0000016
${}_7(4,0)^+_7$	$[1\,5\,0]^+_0$	−0.01251037501	0.00021249120	−0.546555	53.7365	117.1581	0.000531544	0.000354625
${}_7(4,0)^+_8$	$[1\,5\,0]^+_1$	−0.01111082414	0.00011967383	−0.563975	58.7599	160.9299	0.000052737	0.000177156
${}_7(4,0)^+_9$	$[1\,5\,0]^+_2$	−0.01062958229	0.00008096584	−0.564235	58.8726	218.7823	−0.000022478	0.000184679
${}_7(4,0)^+_{10}$	$[1\,5\,0]^+_3$	−0.01041263759	0.00004817646	−0.567999	58.2036	301.4518	0.000018316	0.000169967
${}_7(4,0)^+_{11}$	$[1\,5\,0]^+_4$	−0.0103072411	0.0000241440	−0.562267	57.719	427.312	0.000062500	0.000095705
${}_7(4,0)^+_{12}$	$[1\,5\,0]^+_5$	−0.010254288	0.000011404	−0.56316	57.83	626.57	0.00004313	0.00004130
${}_7(2,0)^+_7$	$[2\,4\,0]^+_0$	−0.01154025645	0.00017511818	−0.315414	60.6512	111.1057	0.000785337	0.000222574
${}_7(2,0)^+_8$	$[2\,4\,0]^+_1$	−0.01050855234	0.00005517383	−0.315819	61.0785	183.0693	0.000218059	0.000152303
${}_7(2,0)^+_9$	$[2\,4\,0]^+_2$	−0.01028393198	0.00001626733	−0.293088	59.8942	317.3280	0.000071544	0.000049280
${}_7(0,0)^+_7$	$[3\,3\,0]^+_0$	−0.01075799323	0.00079933509	−0.018869	55.8531	67.2973	0.004598373	−0.000762021
${}_7(0,0)^+_8$	$[3\,3\,0]^+_1$	−0.01032434054	0.00006491491	−0.135839	66.7767	117.3769	0.000763760	0.000302251
shape		−0.01012995	0.00008913	−0.0346	62.0	189.8	−0.000007	−0.000222
shape		−0.009597985	0.000991857	0.08124	61.46	104.56	0.0004137	−0.0014476
shape		−0.00907232272	0.00029514929	0.002370	72.9972	95.6482	0.002058014	−0.000694991
shape		−0.008565870	0.002476991	−0.24117	47.334	63.534	0.0098318	−0.0009272
${}_8(7,0)^+_8$	$[0\,7\,0]^+_0$	−0.0102536[a]	0.0001506	—	—	—	0.00057	0.00051
${}_8(7,0)^+_9$	$[0\,7\,0]^+_1$	−0.00910889026	0.00011774326	−0.861145	71.7287	195.1685	−0.0000925997	0.000441813
${}_8(7,0)^+_{10}$	$[0\,7\,0]^+_2$	−0.0086317289	0.0000856070	−0.865244	71.8982	233.3368	0.000175506	0.000446169
${}_8(7,0)^+_{11}$	$[0\,7\,0]^+_3$	−0.00834678699	0.00002696759	−0.868319	73.0913	283.5529	0.000299639	0.000066835
${}_8(7,0)^+_{12}$	$[0\,7\,0]^+_4$	−0.00816432312	0.00000073759	−0.868539	74.2107	334.4941	0.000171613	0.000001804
${}_8(7,0)^+_{13}$	$[0\,7\,0]^+_5$	−0.00804234703	0.00000651028	−0.868385	74.470	427.490	0.000010473	−0.000006560
${}_8(7,0)^+_{14}$	$[0\,7\,0]^+_6$	−0.0079554247	0.0000110929	−0.868822	74.474	562.270	−0.000047285	−0.000047508
${}_8(7,0)^+_{15}$	$[0\,7\,0]^+_7$	−0.007899421	0.000010345	−0.867490	75.14	732.42	−0.000054548	−0.000067272
${}_8(7,0)^+_{16}$	$[0\,7\,0]^+_8$	−0.00786490	0.00000794	−0.869405	73.8	956.4	−0.0000433	−0.0000732
${}_8(7,0)^+_{17}$	$[0\,7\,0]^+_9$	−0.0078440	0.0000055	−0.87043	—	—	−0.000024	−0.000067
${}_8(5,0)^+_8$	$[1\,6\,0]^+_0$	−0.00972110856	0.00015987162	−0.596161	67.8105	154.1427	0.000434275	0.000280379
${}_8(5,0)^+_9$	$[1\,6\,0]^+_1$	−0.00868457123	0.00010984610	−0.610427	75.2737	197.5833	0.000022177	0.000174044
${}_8(5,0)^+_{10}$	$[1\,6\,0]^+_2$	−0.00830000761	0.00009194699	−0.615034	76.8276	239.6108	0.000076787	0.000288097
${}_8(5,0)^+_{11}$	$[1\,6\,0]^+_3$	−0.00810469486	0.00004491821	−0.619626	75.0017	311.9291	0.000209032	0.000100377
${}_8(5,0)^+_{12}$	$[1\,6\,0]^+_4$	−0.00797854403	0.00001457179	−0.614326	75.727	421.197	0.000123063	−0.000003512
${}_8(5,0)^+_{13}$	$[1\,6\,0]^+_5$	−0.00790395469	0.00000455930	−0.617630	74.96	572.10	0.00006344	−0.00000926
${}_8(5,0)^+_{14}$	$[1\,6\,0]^+_6$	−0.00786255635	0.00000157196	−0.617008	74.94	777.52	0.000035261	−0.000004752
${}_8(5,0)^+_{15}$	$[1\,6\,0]^+_7$	−0.007839733	0.000000560	−0.6146	75.	1059.	0.00001944	−0.00000255
${}_8(3,0)^+_8$	$[2\,5\,0]^+_0$	−0.00908634696	0.00016554571	−0.408038	74.5773	154.6859	0.000243550	0.000193234
${}_8(3,0)^+_9$	$[2\,5\,0]^+_1$	−0.00823322420	0.00006533947	−0.382333	75.9060	212.6560	0.000184955	0.000002852
${}_8(3,0)^+_{10}$	$[2\,5\,0]^+_2$	−0.00797766268	0.00003712890	−0.383477	77.4826	316.4644	0.000073383	0.000038404
${}_8(3,0)^+_{11}$	$[2\,5\,0]^+_3$	−0.00787817089	0.00001819609	−0.36680	77.170	469.806	0.000034387	0.000020233
${}_8(3,0)^+_{12}$	$[2\,5\,0]^+_4$	−0.007836762	0.000008035	−0.3559	77.0	743.0	0.0000102	0.0000104
${}_8(1,0)^+_8$	$[3\,4\,0]^+_0$	−0.00836289136	0.00008445004	−0.215543	83.4332	143.7768	0.000434394	−0.000064415
${}_8(1,0)^+_9$	$[3\,4\,0]^+_1$	−0.00785035753	0.00001255004	−0.199970	78.894	318.932	0.000160016	0.000022374

Table 3. *Continued.*

state		E_{R}	$\Gamma/2$	$\langle\cos\theta_{12}\rangle$	$\langle r_<\rangle$	$\langle r_>\rangle$	$\mathrm{Re}\langle\langle \mathbf{p}_1\cdot\mathbf{p}_2\rangle\rangle$	$\mathrm{Im}\langle\langle \mathbf{p}_1\cdot\mathbf{p}_2\rangle\rangle$
shape		−0.0073021921	0.0005128598	−0.041819	79.5485	90.7041	0.003716462	−0.000695257
shape		−0.006965845	0.000961105	0.086253	85.261	139.631	0.00077093	−0.00106547
shape		−0.00648176489	0.00030275588	−0.018432	98.9791	123.0143	0.002101727	−0.000761046
$_9(8,0)^+_9$	$[0\,8\,0]^+_0$	−0.00813[a]	0.00012	—	—	—	0.00045	0.00037
$_9(8,0)^+_{10}$	$[0\,8\,0]^+_1$	−0.00728676175	0.00010354564	−0.875349	89.9565	240.0685	−0.000065714	0.000400026
$_9(8,0)^+_{11}$	$[0\,8\,0]^+_2$	−0.00693111930	0.00007353751	−0.879699	90.1350	277.5412	0.000258597	0.000356468
$_9(8,0)^+_{12}$	$[0\,8\,0]^+_3$	−0.00670216083	0.00001058140	−0.881878	91.3199	321.8195	0.000274313	0.000003773
$_9(8,0)^+_{13}$	$[0\,8\,0]^+_4$	−0.00654665844	0.00000663355	−0.881368	93.8607	377.5739	0.000045563	0.000005680
$_9(8,0)^+_{14}$	$[0\,8\,0]^+_5$	−0.0064185679	0.0000249144	−0.881786	93.7024	492.7618	−0.000144794	−0.000144146
$_9(8,0)^+_{15}$	$[0\,8\,0]^+_6$	−0.0063399669	0.0000617298	−0.881584	102.924	288.706	−0.00055379	0.00095612
$_9(8,0)^+_{16}$	$[0\,8\,0]^+_7$	−0.0063130645	0.0000219591	−0.884036	93.952	713.504	0.00033358	−0.00006607
$_9(8,0)^+_{17}$	$[0\,8\,0]^+_8$	−0.0062617104	0.0000096578	−0.883301	94.360	837.594	0.00010166	0.00000140
$_9(8,0)^+_{18}$	$[0\,8\,0]^+_9$	−0.006230045	0.000005088	−0.883560	94.18	1038.88	0.00005013	0.00000217
$_9(6,0)^+_9$	$[1\,7\,0]^+_0$	−0.007765594	0.000127338	−0.63580	84.166	196.488	0.00036463	0.00025555
$_9(6,0)^+_{10}$	$[1\,7\,0]^+_1$	−0.00697828789	0.00009853151	−0.647235	92.9740	241.2936	−0.000024710	0.000181432
$_9(6,0)^+_{11}$	$[1\,7\,0]^+_2$	−0.00668504636	0.00008433047	−0.643709	97.3903	273.1841	0.000163469	0.000259327
$_9(6,0)^+_{12}$	$[1\,7\,0]^+_3$	−0.00650760052	0.00002470166	−0.658697	93.8573	349.2617	0.000200530	0.000010622
$_9(6,0)^+_{13}$	$[1\,7\,0]^+_4$	−0.00638268094	0.00000207533	−0.658149	94.9479	428.5437	0.000113673	−0.000002776
$_9(6,0)^+_{14}$	$[1\,7\,0]^+_5$	−0.00630287289	0.00000131428	−0.656762	94.9377	552.3727	0.000048073	0.000006949
$_9(6,0)^+_{15}$	$[1\,7\,0]^+_6$	−0.00625092121	0.00000250168	−0.656959	94.7538	731.1280	0.000017926	0.000000352
$_9(6,0)^+_{16}$	$[1\,7\,0]^+_7$	−0.0062190464	0.0000022486	−0.657955	94.338	961.233	0.000008761	−0.000002674
$_9(6,0)^+_{17}$	$[1\,7\,0]^+_8$	−0.00620007	0.00000157	−0.6586	93.	1263.	0.000005	−0.000002
$_9(4,0)^+_9$	$[2\,6\,0]^+_0$	−0.00734671122	0.00012535592	−0.434231	93.1497	187.2097	0.000346657	0.000162988
$_9(4,0)^+_{10}$	$[2\,6\,0]^+_1$	−0.00665273669	0.00007934639	−0.460419	96.8096	252.8660	0.000063012	0.000097099
$_9(4,0)^+_{11}$	$[2\,6\,0]^+_2$	−0.00640953938	0.00008060794	−0.460311	101.2435	285.0239	−0.000052822	0.000259554
$_9(4,0)^+_{12}$	$[2\,6\,0]^+_3$	−0.00632260460	0.00004318780	−0.450194	95.3809	397.3053	0.000145014	0.000074408
$_9(4,0)^+_{13}$	$[2\,6\,0]^+_4$	−0.00625231743	0.00001389175	−0.441502	96.9451	559.3923	0.000077805	−0.000014424
$_9(4,0)^+_{14}$	$[2\,6\,0]^+_5$	−0.00621218306	0.00000542794	−0.44349	96.72	797.90	0.00003718	−0.00000605
$_9(4,0)^+_{15}$	$[2\,6\,0]^+_6$	−0.00619241	0.00000212	−0.4353	96.	1116.	0.000018	−0.000004
$_9(2,0)^+_9$	$[3\,5\,0]^+_0$	−0.00685967040	0.00010155532	−0.270290	102.1229	179.4379	0.000581210	0.000079823
$_9(2,0)^+_{10}$	$[3\,5\,0]^+_1$	−0.00633911397	0.00004065403	−0.279203	105.6416	271.3966	0.000235191	0.000162177
$_9(2,0)^+_{11}$	$[3\,5\,0]^+_2$	−0.00621515959	0.00001120879	−0.238081	99.9964	460.1576	0.000049854	0.000037105
$_9(0,0)^+_9$	$[4\,4\,0]^+_0$	−0.00751392408	0.00007060016	−0.050773	91.4855	158.4665	0.000705895	−0.000041340
$_9(0,0)^+_{10}$	$[4\,4\,0]^+_1$	−0.00624954679	0.00005227339	−0.125631	110.4143	182.0725	0.000484239	0.000162704
shape		−0.00611213	0.00003996	−0.0556	103.3	308.7	0.0000725	−0.0001353
shape		−0.0058153394	0.0003958043	0.025836	104.340	180.072	0.00036907	−0.00073119
shape		−0.00525362531	0.00031986319	−0.052478	111.7998	122.2470	0.002901509	−0.000207756
$_{10}(9,0)^+_{10}$	$[0\,9\,0]^+_0$	−0.0064[b]	—	—	—	—	—	—
$_{10}(9,0)^+_{11}$	$[0\,9\,0]^+_1$	−0.00596466502	0.00009162464	−0.886948	110.0518	289.9356	−0.000037491	0.000369900
$_{10}(9,0)^+_{12}$	$[0\,9\,0]^+_2$	−0.00569614418	0.00006056954	−0.891137	109.2893	328.7529	0.000298546	0.000262688
$_{10}(9,0)^+_{13}$	$[0\,9\,0]^+_3$	−0.00551076975	0.00000270672	−0.892589	111.8824	368.3672	0.000217804	0.000003120
$_{10}(9,0)^+_{14}$	$[0\,9\,0]^+_4$	−0.0053686477	0.0000177072	−0.891699	115.8120	443.1426	−0.000053358	−0.000045599
$_{10}(9,0)^+_{15}$	$[0\,9\,0]^+_5$	−0.005263711	0.000072975	−0.891935	126.373	329.429	−0.00037680	0.00075085
$_{10}(9,0)^+_{16}$	$[0\,9\,0]^+_6$	−0.0052241845	0.0000242751	−0.895397	112.352	620.608	0.00029163	−0.00005597
$_{10}(9,0)^+_{17}$	$[0\,9\,0]^+_7$	−0.0051489679	0.0000087590	−0.887418	108.332	717.368	0.000083371	−0.000000642
$_{10}(9,0)^+_{18}$	$[0\,9\,0]^+_8$	−0.0051009033	0.0000036484	−0.893600	116.869	862.205	0.000046404	0.000000714
$_{10}(9,0)^+_{19}$	$[0\,9\,0]^+_9$	−0.0050685228	0.0000015761	−0.894614	116.079	1047.208	0.000026723	0.000001065
$_{10}(9,0)^+_{20}$	$[0\,9\,0]^+_{10}$	−0.00504660	0.00000069	−0.89497	114.	1276.	0.000016	0.000002
$_{10}(7,0)^+_{10}$	$[1\,8\,0]^+_0$	−0.0062[b]	—	—	—	—	—	—
$_{10}(7,0)^+_{11}$	$[1\,8\,0]^+_1$	−0.00573389850	0.00009167609	−0.677415	114.4299	288.9163	−0.000021151	0.000225552
$_{10}(7,0)^+_{12}$	$[1\,8\,0]^+_2$	−0.0055101680	0.0000727346	−0.684782	116.0909	323.1091	0.000230443	0.000239012
$_{10}(7,0)^+_{13}$	$[1\,8\,0]^+_3$	−0.00535290956	0.00001002314	−0.690768	114.2385	389.0233	0.000176426	−0.000005209
$_{10}(7,0)^+_{14}$	$[1\,8\,0]^+_4$	−0.00523860854	0.00000283845	−0.688813	117.3978	467.8580	0.000071117	0.000012792

Table 3. *Continued.*

state		E_R	$\Gamma/2$	$\langle\cos\theta_{12}\rangle$	$\langle r_<\rangle$	$\langle r_>\rangle$	$\mathrm{Re}\langle\langle \mathbf{p}_1\cdot\mathbf{p}_2\rangle\rangle$	$\mathrm{Im}\langle\langle \mathbf{p}_1\cdot\mathbf{p}_2\rangle\rangle$
${}_{10}(7,0)^+_{15}$	$[1\,8\,0]^+_5$	−0.00515225718	0.00000826867	−0.695785	119.4937	614.6629	0.000023022	−0.000018432
${}_{10}(7,0)^+_{16}$	$[1\,8\,0]^+_6$	−0.00509369202	0.00000775471	−0.690063	116.7021	795.5313	0.000016688	−0.000030758
${}_{10}(7,0)^+_{17}$	$[1\,8\,0]^+_7$	−0.00505766909	0.00000521920	−0.687936	117.160	1009.460	0.000019712	−0.000021186
${}_{10}(7,0)^+_{18}$	$[1\,8\,0]^+_8$	−0.0050473800	0.0001010142	−0.687096	131.974	303.857	−0.000126820	0.000580887
${}_{10}(7,0)^+_{19}$	$[1\,8\,0]^+_9$	−0.005035794	0.000003157	−0.6881	114.	1272.	0.000015	−0.000012
${}_{10}(5,0)^+_{10}$	$[2\,7\,0]^+_0$	−0.0060455938	0.0001000992	−0.481919	109.8371	234.5029	0.00029505	0.00012570
${}_{10}(5,0)^+_{11}$	$[2\,7\,0]^+_1$	−0.00549324160	0.00007381984	−0.498007	118.9031	293.8205	0.000067182	0.000088377
${}_{10}(5,0)^+_{12}$	$[2\,7\,0]^+_2$	−0.00530690756	0.00007713107	−0.495626	120.7225	317.4621	0.000184202	0.000186436
${}_{10}(5,0)^+_{13}$	$[2\,7\,0]^+_3$	−0.00519983265	0.00002196045	−0.503520	117.8278	433.1554	0.000143517	−0.000011722
${}_{10}(5,0)^+_{14}$	$[2\,7\,0]^+_4$	−0.00511609341	0.00000350228	−0.495992	119.3901	549.1501	0.000080271	−0.000010366
${}_{10}(5,0)^+_{15}$	$[2\,7\,0]^+_5$	−0.00506688854	0.00000058932	−0.497370	118.4186	720.7342	0.000044000	0.000000231
${}_{10}(5,0)^+_{16}$	$[2\,7\,0]^+_6$	−0.0050382261	0.0000004709	−0.49881	117.91	964.63	0.00002451	0.00000378
${}_{10}(5,0)^+_{17}$	$[2\,7\,0]^+_7$	−0.005021464	0.000000340	−0.488	119.	1283.	0.0000121	0.0000026
${}_{10}(5,0)^+_{18}$	$[2\,7\,0]^+_8$	−0.0050121	0.0000004	−0.492	103.	1737.	0.000005	−0.000001
${}_{10}(3,0)^+_{10}$	$[3\,6\,0]^+_0$	−0.00571201597	0.00010078558	−0.281961	127.1396	211.2606	0.000479865	0.000113932
${}_{10}(3,0)^+_{11}$	$[3\,6\,0]^+_1$	−0.00524051816	0.00004090879	−0.320808	120.7256	313.2870	0.000178666	−0.000016013
${}_{10}(3,0)^+_{12}$	$[3\,6\,0]^+_2$	−0.00509282134	0.00002615484	−0.315213	121.9048	470.1776	0.000073909	0.000023555
${}_{10}(3,0)^+_{13}$	$[3\,6\,0]^+_3$	−0.0050349499	0.0000123691	−0.28019	121.91	675.15	0.00004713	0.00000451
${}_{10}(1,0)^+_{10}$	$[4\,5\,0]^+_0$	−0.00565411766	0.00009578782	−0.081939	123.4942	179.0634	0.000790685	−0.000357167
${}_{10}(1,0)^+_{11}$	$[4\,5\,0]^+_1$	−0.00531016773	0.00004581209	−0.207344	132.9508	221.9836	0.000297138	−0.000011167
${}_{10}(1,0)^+_{12}$	$[4\,5\,0]^+_2$	−0.005022878	0.000008656	−0.19804	123.1	492.1	0.0001153	−0.0000038

[a] Perturber, direct calculation [41–43]

[b] Perturber, estimated position

Table 4. Same as Table 3, but for states of $^1\mathrm{P^o}$ symmetry.

state		E_R	$\Gamma/2$	$\langle\cos\theta_{12}\rangle$	$\langle r_<\rangle$	$\langle r_>\rangle$	$\mathrm{Re}\langle\langle \mathbf{p}_1\cdot\mathbf{p}_2\rangle\rangle$	$\mathrm{Im}\langle\langle \mathbf{p}_1\cdot\mathbf{p}_2\rangle\rangle$
${}_2(1,0)^-_3$	$[0\,1\,0]^-_0$	−0.12604985948	0.00000068419	−0.448412	4.9543	34.3482	0.00069912	−0.00000459
${}_2(1,0)^-_4$	$[0\,1\,0]^-_1$	−0.125035052	0.000000039	−0.446917	4.7935	186.6065	0.000021	−0.000007
${}_2(0,1)^+_2$	$[0\,0\,1]^+_0$	−0.124393557	0.000350504	−0.063674	5.9516	11.6084	0.00241412	−0.00217722
${}_3(2,0)^-_4$	$[0\,2\,0]^-_0$	−0.05857181141	0.00000449363	−0.641551	10.6358	39.6874	0.00148018	0.00003117
${}_3(2,0)^-_5$	$[0\,2\,0]^-_1$	−0.05611640047	0.00000112952	−0.635329	10.7356	90.1585	0.00026362	0.00000740
${}_3(2,0)^-_6$	$[0\,2\,0]^-_2$	−0.055663057	0.000000198	−0.637171	10.81	206.73	0.0000508	0.0000014
${}_3(1,1)^+_3$	$[0\,1\,1]^+_0$	−0.0627167721	0.0005957403	−0.340662	10.7445	22.2336	0.0016597	0.0003285
${}_3(1,1)^+_4$	$[0\,1\,1]^+_1$	−0.0559062460	0.0000355146	−0.339397	10.9878	73.6296	0.0002142	0.0000247
${}_3(1,1)^+_5$	$[0\,1\,1]^+_2$	−0.0555764	0.0000026	−0.331	9.	277.	0.000015	−0.000002
shape		−0.04767516	0.00431197	0.014749	11.1683	20.1125	0.00795	−0.00579
${}_4(3,0)^-_5$	$[0\,3\,0]^-_0$	−0.03429402719	0.00000915162	−0.727544	18.2305	58.1303	0.00119544	0.00006711
${}_4(3,0)^-_6$	$[0\,3\,0]^-_1$	−0.03219830788	0.00000395831	−0.731498	18.9243	100.5821	0.00033358	0.00002678
${}_4(3,0)^-_7$	$[0\,3\,0]^-_2$	−0.03155519623	0.00000136181	−0.719576	18.8682	175.9287	0.00009777	0.00000915
${}_4(3,0)^-_8$	$[0\,3\,0]^-_3$	−0.031349806	0.000000438	−0.73007	18.7	312.3	0.0000329	0.0000031
${}_4(2,1)^+_4$	$[0\,2\,1]^+_0$	−0.03717945790	0.00051677410	−0.479652	18.1071	38.8917	0.001117	0.000956
${}_4(2,1)^+_5$	$[0\,2\,1]^+_1$	−0.03235104573	0.00012063609	−0.493448	19.2409	74.8107	0.0001654	0.0002272
${}_4(2,1)^+_6$	$[0\,2\,1]^+_2$	−0.031497534	0.000032822	−0.497505	19.1447	153.5025	0.000007	0.000120
${}_4(1,0)^-_5$	$[1\,2\,0]^-_0$	−0.03161320952	0.00000298090	−0.273885	19.6541	79.2863	0.00054327	0.00000186
${}_4(0,1)^+_4$	$[1\,1\,1]^+_0$	−0.0313233	0.0000568	−0.140	19.5	65.7	0.0023	0.0001
shape		−0.02950891	0.00329825	0.07091	20.22	34.08	0.00025	−0.00349
shape		−0.02311464	0.00298775	−0.0178	17.01	39.29	0.008854	−0.003818
${}_5(4,0)^-_6$	$[0\,4\,0]^-_0$	−0.02263065147	0.00001181991	−0.779015	27.6962	82.6507	0.00091307	0.00008767
${}_5(4,0)^-_7$	$[0\,4\,0]^-_1$	−0.0210700270	0.0000075306	−0.722680	31.0357	117.1287	0.0004069	0.0000655

Table 4. *Continued.*

state		E_{R}	$\Gamma/2$	$\langle\cos\theta_{12}\rangle$	$\langle r_<\rangle$	$\langle r_>\rangle$	$\mathrm{Re}\langle\langle \mathbf{p}_1\cdot\mathbf{p}_2\rangle\rangle$	$\mathrm{Im}\langle\langle \mathbf{p}_1\cdot\mathbf{p}_2\rangle\rangle$
${}_5(4,0)^-_8$	$[0\,4\,0]^-_2$	−0.0204461387	0.0000032383	−0.785293	29.2750	191.2750	0.0001142	0.0000228
${}_5(4,0)^-_9$	$[0\,4\,0]^-_3$	−0.02018919341	0.00000142399	−0.782842	29.2011	294.5763	0.0000453	0.0000098
${}_5(4,0)^-_{10}$	$[0\,4\,0]^-_4$	−0.02008078	0.00000061	−0.78481	29.5	453.7	0.000020	0.000004
${}_5(3,1)^+_5$	$[0\,3\,1]^+_0$	−0.02451674280	0.00038466422	−0.570017	26.9470	61.1230	0.00077182	0.00080245
${}_5(3,1)^+_6$	$[0\,3\,1]^+_1$	−0.0213297438	0.0001468122	−0.585697	28.9627	95.9553	−0.0000079	0.0002246
${}_5(3,1)^+_7$	$[0\,3\,1]^+_2$	−0.02047120306	0.00006198903	−0.588251	29.5056	155.6960	−0.0000202	0.0001121
${}_5(3,1)^+_8$	$[0\,3\,1]^+_3$	−0.020168827	0.000023724	−0.589554	29.397	258.429	−0.0000060	0.0000469
${}_5(3,1)^+_9$	$[0\,3\,1]^+_4$	−0.02006025	0.00000877	−0.58981	28.	438.	−0.000005	0.000018
${}_5(2,0)^-_6$	$[1\,3\,0]^-_0$	−0.02103170005	0.00000943899	−0.468394	28.8687	93.9226	0.00050532	0.00001322
${}_5(2,0)^-_7$	$[1\,3\,0]^-_1$	−0.02024029718	0.00000302929	−0.395658	30.1413	167.1814	0.00016976	0.00000959
${}_5(2,0)^-_8$	$[1\,3\,0]^-_2$	−0.020056467	0.000000741	−0.3870	30.4	334.2	0.0000423	0.0000025
${}_5(1,1)^+_5$	$[1\,2\,1]^-_0$	−0.02181449120	0.00025324335	−0.251491	31.0913	58.5868	0.00087553	−0.00011962
${}_5(1,1)^+_6$	$[1\,2\,1]^+_1$	−0.020106449	0.000021936	−0.225427	30.8951	148.8443	0.0002162	0.0000233
shape		−0.0197551	0.0003136	−0.062	32.	70.	0.00016	−0.00071
shape		−0.018478927	0.000562917	−0.030766	38.04	51.76	0.0024011	−0.0012644
shape		−0.017266302	0.002941883	0.075028	32.8869	52.9811	0.001496	−0.003411
${}_6(5,0)^-_7$	$[0\,5\,0]^-_0$	−0.0160878815	0.0000129948	−0.813700	38.9890	112.6096	0.0007094	0.0000961
${}_6(5,0)^-_8$	$[0\,5\,0]^-_1$	−0.0149327709	0.0000088882	−0.818259	40.4078	156.2870	0.0002390	0.0000635
${}_6(5,0)^-_9$	$[0\,5\,0]^-_2$	−0.01440259791	0.00000512104	−0.818559	42.1480	219.0886	0.00010894	0.00003747
${}_6(5,0)^-_{10}$	$[0\,5\,0]^-_3$	−0.01414449963	0.00000271930	−0.821040	41.886	311.552	0.00004982	0.00001960
${}_6(5,0)^-_{11}$	$[0\,5\,0]^-_4$	−0.014016832	0.000001405	−0.820711	41.8	442.2	0.0000238	0.0000100
${}_6(4,1)^+_6$	$[0\,4\,1]^+_0$	−0.0173595938	0.0002757828	−0.634035	37.8149	88.0941	0.0006652	0.0006166
${}_6(4,1)^+_7$	$[0\,4\,1]^+_1$	−0.0152060983	0.0001450995	−0.649620	41.6945	123.6457	−0.0000321	0.0002778
${}_6(4,1)^+_8$	$[0\,4\,1]^+_2$	−0.01448349925	0.00008554092	−0.653370	42.3863	175.4877	−0.00005195	0.00022942
${}_6(4,1)^+_9$	$[0\,4\,1]^+_3$	−0.0141626038	0.0000441140	−0.655664	42.10	256.02	−0.0000095	0.0001526
${}_6(4,1)^+_{10}$	$[0\,4\,1]^+_4$	−0.014014549	0.000020979	−0.656763	42.1	379.8	0.0000070	0.0000799
${}_6(3,0)^-_7$	$[1\,4\,0]^-_0$	−0.01511016337	0.00001421216	−0.494614	42.6014	112.9150	0.00052089	0.00004871
${}_6(3,0)^-_8$	$[1\,4\,0]^-_1$	−0.01432433581	0.00000696334	−0.494352	42.9854	177.2240	0.00019923	0.00002148
${}_6(3,0)^-_9$	$[1\,4\,0]^-_2$	−0.01404563317	0.00000277055	−0.439953	42.8352	263.1894	0.00010504	0.00000381
${}_6(2,1)^+_6$	$[1\,3\,1]^+_0$	−0.0158735282	0.0002449534	−0.347047	43.5503	83.0471	0.0008997	0.0003149
${}_6(2,1)^+_7$	$[1\,3\,1]^+_1$	−0.01431564622	0.00006955765	−0.351338	44.4559	142.8225	0.00023693	0.00015729
${}_6(2,1)^+_8$	$[1\,3\,1]^+_2$	−0.01399404647	0.00001743332	−0.325108	43.381	256.313	0.00010564	0.00001279
${}_6(1,0)^-_7$	$[2\,3\,0]^-_0$	−0.01406344209	0.00000403272	−0.2647	43.96	160.99	0.00037951	0.00001060
${}_6(0,1)^+_6$	$[2\,2\,1]^+_0$	−0.01400286586	0.00006937239	−0.13866	48.09	95.25	0.00094817	0.00046503
shape		−0.01314779358	0.00070197580	−0.00310	47.1392	83.3798	0.000569	−0.001108
shape		−0.01190611905	0.00074381997	−0.001393	54.0599	75.6763	0.00206603	−0.00168826
shape		−0.010914763	0.002237373	0.045390	48.9851	74.6379	0.002255	−0.002934
${}_7(6,0)^-_8$	$[0\,6\,0]^-_0$	−0.01203774958	0.00001327045	−0.838803	52.0837	147.8503	0.00056632	0.00009683
${}_7(6,0)^-_9$	$[0\,6\,0]^-_1$	−0.01117514783	0.00001044212	−0.843187	54.6393	193.4675	0.00020153	0.00007456
${}_7(6,0)^-_{10}$	$[0\,6\,0]^-_2$	−0.01073367888	0.00000768850	−0.747698	53.3378	240.9868	0.00011477	0.00001611
${}_7(6,0)^-_{11}$	$[0\,6\,0]^-_3$	−0.01049929197	0.00000410896	−0.845529	56.8869	343.4063	0.00004868	0.00003028
${}_7(6,0)^-_{12}$	$[0\,6\,0]^-_4$	−0.01036878543	0.00000238492	−0.846745	56.748	461.278	0.00002599	0.00001761
${}_7(6,0)^-_{13}$	$[0\,6\,0]^-_5$	−0.01029626	0.00000134	−0.84705	57.	623.	−0.00008	0.00007
${}_7(5,1)^+_7$	$[0\,5\,1]^+_0$	−0.01292250777	0.00020356134	−0.681687	50.1114	120.5662	0.00054553	0.00047923
${}_7(5,1)^+_8$	$[0\,5\,1]^+_1$	−0.0114148112	0.0001304375	−0.694756	55.8905	157.4325	−0.0000515	0.0002769
${}_7(5,1)^+_9$	$[0\,5\,1]^+_2$	−0.01084916591	0.00009448720	−0.698552	57.6997	201.4903	0.00000122	0.00033361
${}_7(5,1)^+_{10}$	$[0\,5\,1]^+_3$	−0.0105622582	0.0000509551	−0.703854	56.765	266.883	0.0001462	0.0002008
${}_7(5,1)^+_{11}$	$[0\,5\,1]^+_4$	−0.0104003605	0.0000221426	−0.704675	56.75	365.91	0.0001305	0.0000616

Table 4. *Continued.*

state		E_{R}	$\Gamma/2$	$\langle\cos\theta_{12}\rangle$	$\langle r_<\rangle$	$\langle r_>\rangle$	$\mathrm{Re}\langle\langle\mathbf{p}_1\cdot\mathbf{p}_2\rangle\rangle$	$\mathrm{Im}\langle\langle\mathbf{p}_1\cdot\mathbf{p}_2\rangle\rangle$
$_7(5,1)^+_{12}$	$[0\,5\,1]^+_5$	−0.010309257	0.000009283	−0.705147	56.5	507.3	0.000074	0.000013
$_7(4,0)^-_8$	$[1\,5\,0]^-_0$	−0.01140241316	0.00001539359	−0.557433	56.3532	145.7302	0.00042733	0.00005672
$_7(4,0)^-_9$	$[1\,5\,0]^-_1$	−0.01074023868	0.00000911432	−0.637595	62.2941	216.0911	0.00020985	0.00007308
$_7(4,0)^-_{10}$	$[1\,5\,0]^-_2$	−0.01044670804	0.00000512502	−0.559912	57.9619	297.5991	0.00008349	0.00001796
$_7(4,0)^-_{11}$	$[1\,5\,0]^-_3$	−0.0103155677	0.0000025025	−0.54179	58.09	425.83	0.0000375	0.0000084
$_7(4,0)^-_{12}$	$[1\,5\,0]^-_4$	−0.0102562	0.0000012	−0.5571	58.	646.	0.00022	0.00018
$_7(3,1)^+_7$	$[1\,4\,1]^+_0$	−0.01202201586	0.00020910186	−0.424515	56.1814	115.5648	0.00048697	0.00022332
$_7(3,1)^+_8$	$[1\,4\,1]^+_1$	−0.01078577237	0.00008523730	−0.428098	57.4089	169.1783	0.00016506	0.00002920
$_7(3,1)^+_9$	$[1\,4\,1]^+_2$	−0.01042776763	0.00004443547	−0.428121	59.0303	255.9665	0.00006265	0.00004721
$_7(3,1)^+_{10}$	$[1\,4\,1]^+_3$	−0.0102910985	0.0000201843	−0.42183	58.58	396.32	0.0000260	0.0000259
$_7(2,0)^-_8$	$[2\,4\,0]^-_0$	−0.01068902214	0.00000985401	−0.339103	58.8302	157.5144	0.00034508	0.00001551
$_7(2,0)^-_9$	$[2\,4\,0]^-_1$	−0.01032802465	0.00000348696	−0.315956	59.543	271.519	0.00013922	0.00000972
$_7(2,0)^-_{10}$	$[2\,4\,0]^-_2$	−0.01023445	0.00000096	−0.283	60.	492.	0.00005	−0.00002
$_7(1,1)^+_7$	$[2\,3\,1]^+_0$	−0.01095174403	0.00011514216	−0.220870	62.8698	111.3130	0.00055793	−0.00015547
$_7(1,1)^+_8$	$[2\,3\,1]^+_1$	−0.010249298	0.000013960	−0.195	60.	248.	0.000180	0.000026
shape		−0.010062644	0.000077496	−0.07994	62.7	150.9	0.000233	−0.000305
shape		−0.00969838226	0.00012724354	−0.047538	70.7283	112.2243	0.00109352	−0.00032933
shape		−0.0091560112	0.0007807020	0.022013	66.6461	107.5651	0.000869	−0.001159
shape		−0.00900978	0.00161141	0.1284	63.58	103.22	0.000554	−0.001934
shape		−0.00836693326	0.00062839901	−0.013773	77.2311	90.2745	0.00279719	0.00077291
$_8(7,0)^-_9$	$[0\,7\,0]^-_0$	−0.00935212825	0.00001303828	−0.857870	66.9979	188.2829	0.00046388	0.00009332
$_8(7,0)^-_{10}$	$[0\,7\,0]^-_1$	−0.00869522826	0.00001138507	−0.861724	70.7046	236.2490	0.00017070	0.00008048
$_8(7,0)^-_{11}$	$[0\,7\,0]^-_2$	−0.00833548958	0.00000815308	−0.863241	70.8277	301.8585	0.00007925	0.00005849
$_8(7,0)^-_{12}$	$[0\,7\,0]^-_3$	−0.00812663454	0.00000546777	−0.862370	74.8330	383.7732	0.00004784	0.00004110
$_8(7,0)^-_{13}$	$[0\,7\,0]^-_4$	−0.00800212564	0.00000345218	−0.865167	73.907	496.031	0.00002809	0.00002609
$_8(7,0)^-_{14}$	$[0\,7\,0]^-_5$	−0.007927367	0.000002148	−0.86585	73.5	639.9	0.000016	0.000016
$_8(6,1)^+_8$	$[0\,6\,1]^+_0$	−0.009989563	0.000157728	−0.718376	64.359	158.197	0.000469	0.000399
$_8(6,1)^+_9$	$[0\,6\,1]^+_1$	−0.00889432916	0.00011606991	−0.728874	71.9518	196.8732	−0.00006694	0.00028538
$_8(6,1)^+_{10}$	$[0\,6\,1]^+_2$	−0.0084660491	0.0000929378	−0.697060	78.9094	227.6360	0.00015684	0.00033343
$_8(6,1)^+_{11}$	$[0\,6\,1]^+_3$	−0.00822209088	0.00003620570	−0.739480	73.2869	296.8845	0.00024046	0.00008421
$_8(6,1)^+_{12}$	$[0\,6\,1]^+_4$	−0.00806288524	0.00000657637	−0.740383	73.7541	374.8813	0.00015089	−0.00000975
$_8(6,1)^+_{13}$	$[0\,6\,1]^+_5$	−0.0079650416	0.0000003612	−0.740931	74.07	477.57	0.0000780	0.0000017
$_8(6,1)^+_{14}$	$[0\,6\,1]^+_6$	−0.00790390	0.00000096	−0.73985	74.2	633.2	0.000033	−0.000001
$_8(5,0)^-_9$	$[1\,6\,0]^-_0$	−0.00891842744	0.00001529364	−0.606028	71.9086	184.3708	0.00035780	0.00005943
$_8(5,0)^-_{10}$	$[1\,6\,0]^-_1$	−0.00837092107	0.00001135374	−0.609104	73.4440	244.0934	0.00014589	0.00004126
$_8(5,0)^-_{11}$	$[1\,6\,0]^-_2$	−0.00810607455	0.00000714877	−0.612228	75.4068	328.5004	0.00008334	0.00002719
$_8(5,0)^-_{12}$	$[1\,6\,0]^-_3$	−0.00796793017	0.00000409729	−0.611130	75.179	447.565	0.00004255	0.00001557
$_8(5,0)^-_{13}$	$[1\,6\,0]^-_4$	−0.007895008	0.000002283	−0.6031	75.5	606.1	0.000021	0.000009
$_8(4,1)^+_8$	$[1\,5\,1]^+_0$	−0.00941356442	0.00016073759	−0.480163	71.5186	150.4632	0.00040648	0.00022041
$_8(4,1)^+_9$	$[1\,5\,1]^+_1$	−0.00845419790	0.00009287734	−0.533579	73.2184	209.0840	0.00001494	0.00012806
$_8(4,1)^+_{10}$	$[1\,5\,1]^+_2$	−0.00812168146	0.00007568056	−0.498253	77.4977	262.5305	−0.00002106	0.00016528
$_8(4,1)^+_{11}$	$[1\,5\,1]^+_3$	−0.0079787602	0.0000511767	−0.506051	76.43	331.07	0.0001003	0.0001901
$_8(4,1)^+_{12}$	$[1\,5\,1]^+_4$	−0.0079018534	0.0000221925	−0.49463	75.75	481.91	0.0001083	0.0000307
$_8(3,0)^-_9$	$[2\,5\,0]^-_0$	−0.00843337946	0.00001319170	−0.392599	78.5815	185.0395	0.00034108	0.00003145
$_8(3,0)^-_{10}$	$[2\,5\,0]^-_1$	−0.00804995542	0.00000703818	−0.385860	77.6197	272.5743	0.00015415	0.00001641
$_8(3,0)^-_{11}$	$[2\,5\,0]^-_2$	−0.00790278380	0.00000303459	−0.347285	76.58	386.56	0.00009370	0.00000420
$_8(2,1)^+_8$	$[2\,4\,1]^+_0$	−0.00873839078	0.00013205482	−0.287598	80.2244	142.9168	0.00064428	0.00014114
$_8(2,1)^+_9$	$[2\,4\,1]^+_1$	−0.00802621203	0.00004516041	−0.285639	80.3730	228.4842	0.00019132	0.00014922
$_8(2,1)^+_{10}$	$[2\,4\,1]^+_2$	−0.007867113	0.000013345	−0.2688	78.3	397.7	0.000053	0.000036
$_8(1,0)^-_9$	$[3\,4\,0]^-_0$	−0.00791587542	0.00000411898	−0.233280	79.167	249.537	0.00028184	0.00001127
$_8(0,1)^+_8$	$[3\,3\,1]^+_0$	−0.00789898264	0.00006017797	−0.133223	86.737	150.522	0.00052204	0.00033340